ACS APPLIED NANO MATERIALS

www.acsanm.org Article

Multiscale Photonic Crystal Enhanced Core−Shell Plasmonic Nanomaterial for Rapid Vapor-Phase Detection of Explosives

Kenneth J. Squire, Kundan Sivashanmugan, Boxin Zhang, Joseph Kraai, Gregory Rorrer, and Alan X. Wang*

Cite This: https://dx.doi.org/10.1021/acsanm.9b02399 Read Online

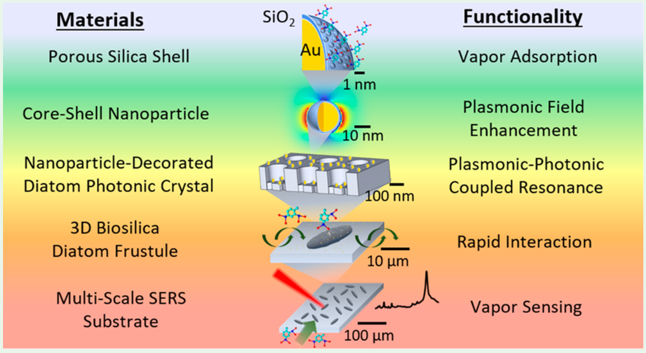

ABSTRACT: Surface-enhanced Raman scattering (SERS) has started to attract attention in vapor sensing; however, practical applications require shorter response time and better sensitivity. Herein, we report a facile multiscale SERS substrate for trace-level detection of vapors using a portable Raman spectrometer through the synergistic integration of biologically fabricated diatom photonic crystals and gold−silica core−shell nanoparticles. The multiscale substrate is composed of (1) a micrometer-scaled, 3-dimensional, diatom biosilica frustule enabling efficient vapor−substrate interaction for rapid sensing, (2) periodic pores, on the order of 100 nm, inducing plasmonic-photonic coupled resonances for enhanced SERS signals, (3) gold nanoparticle cores, with a diameter on the order of 10 nm, contributing plasmonic field enhancements, and (4) porous 1 nm thick silica core−shells enabling analyte vapor adsorption and concentration. The combination of the hierarchal, multiscale features results in a SERS substrate capable of rapid and sensitive detection of target vapors in air. The multiscale substrate's functionality is characterized using the polycyclic aromatic hydrocarbon pyrene, and the contribution from each scale is verified by using a stagnant vapor chamber. The sensor equilibrates in only 3 min, and detection is achieved down to 1 ppm. The sensor is then applied to the detection of explosive 2,4-dinitrotoluene vapor below 100 ppb in an airflow chamber to replicate practical detection conditions, achieving detection in under 3 min at room temperature and under 1 min when heated. This work successfully demonstrates detection of explosive vapor and represents a significant advancement toward widespread vapor sensing via SERS.

KEYWORDS: *multiscale nanomaterial, photonic crystals, core−shell nanoparticles, explosives detection, surface-enhanced Raman scattering*

1. INTRODUCTION

Surface-enhanced Raman spectroscopy (SERS) is an appealing optical detection technique due to its capacity for rapid sensing, multiplex detection, and high sensitivity, capable of achieving single molecule detection.[1,2] Because of the many benefits of SERS sensing, its implementation to the detection of vapor analytes has been explored for several years,[3−6] particularly for the detection of explosives.[7] However, improved response time and sensitivity are required for practical detections. The natural diffusion of the analyte vapor to a substrate is slow and hinders the response time of the sensor. For example, Chou et al. utilized a laser ablation fabricated gold nanostructured substrate to detect explosive 2,4-dinitrotoluene (DNT) vapor but required 18 h of analyte interaction.[8] To improve the response time, "flow-through"[9,10] and "flow-over"[11] type sensors have been employed to reduce vapor diffusion time. Piorek and co-workers fabricated an open microfluidic channel, flowing plasmonic nanoparticles (NPs) to capture explosive DNT vapor across the open channel. However, this required a constant supply of flowing NPs, and the complicated fluidic vapor setup renders great difficulty in implementation.[11] Similarly, other applications requiring external circulation apparatuses also add complexity and difficulty to sensing setups.

Sensitive detection of trace levels of the explosive vapor enables remote and accurate sensing. High SERS sensitivity can be achieved through the rational design and fabrication of novel SERS substrates such as Demeritte's detection 100 fM 2,4,6-trinitrotoluene (TNT) in solution by using a single-walled carbon nanotube functionalized with popcorn-shaped gold nanoparticles.[12] However, the plasmonic field enhancements accompanying the SERS substrates are localized effects

Received: December 5, 2019
Accepted: January 29, 2020
Published: January 29, 2020

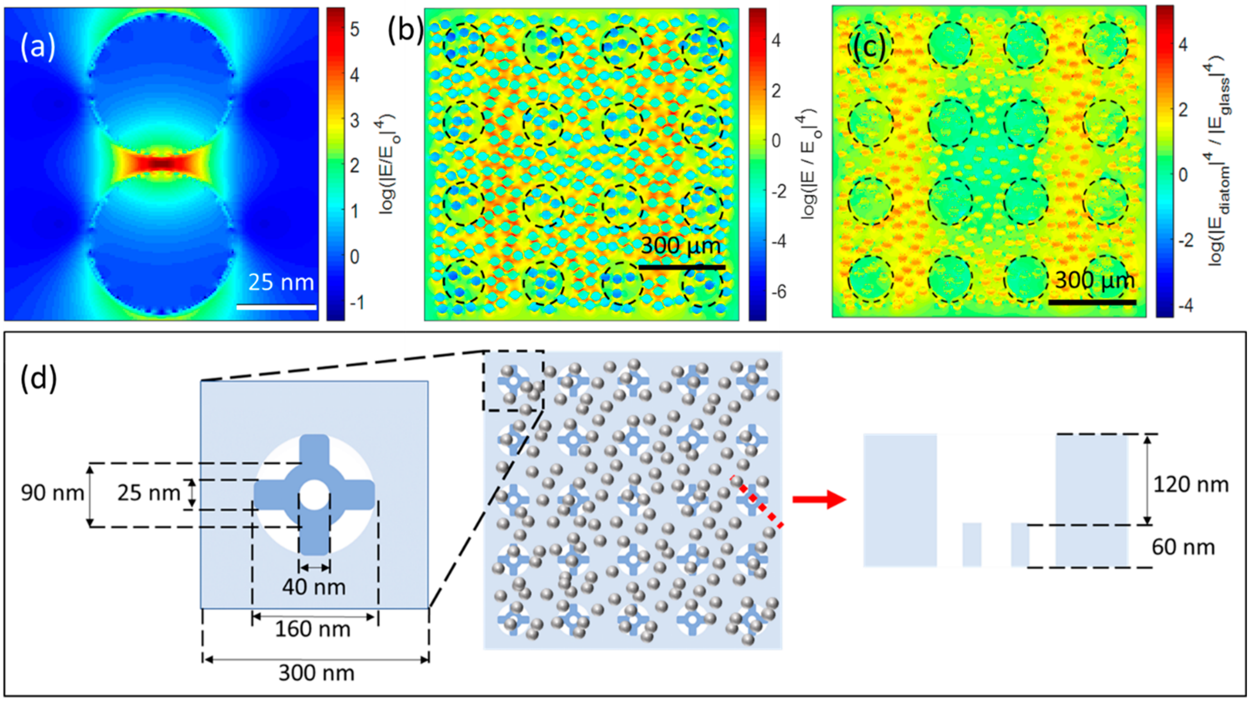

Figure 1. FDTD simulation of plasmonic-enhanced field between two Au@SiO$_2$ NPs (a). The NPs are randomly dispersed on a glass substrate and on a simulated diatom structure with the enhanced electromagnetic field ($|E^4/E_0|$) (b) and additional SERS enhancement from diatom plotted both on a log scale (c). The simulated structure is shown with expanded regions highlighting the scale of the structure (d).

and, without analyte adsorption capabilities, are dependent upon vapor diffusion and condensation. Vapor adsorption allows for the capture and concentration of the target molecule within sensing regions and ensures the stability of the measurement. Improved vapor adsorption has been attained through substrate chemical functionalization[13,14] and utilization of 3-dimensional (3D) materials.[15,16] Wang et al. fabricated rationally designed nanocluster arrays, and Sylvia et al. prepared a roughened gold substrate for explosive vapor detection. Detection was achieved down to 10 ppt and 5 ppb, respectively. However, both required wetting the substrate with sodium hydroxide to increase the binding affinity and enable analyte adsorption, resulting in a sensing process that is more involved and tedious.[13,14] Our group has previously achieved detection of attogram levels of TNT, but this was solution-based detection, requiring inkjet printing for sample concentration.[17] A vapor sensor with strong analyte adsorption is needed to achieve rapid response and high sensitivity for practical engineering applications.

Multiscale materials have extended the horizon of SERS sensing.[18,19] Kreno et al. fabricated a porous metal−organic framework over a silver "film-on-nanoparticles" structure to increase surface area and analyte trapping while also enhancing SERS.[4] Multiscale gold (Au)−areole structures, mimicking the areole of cactus, was created by Li et al. on a superhydrophobic−superhydrophobic substrate, demonstrating effective analyte concentration to a SERS hot spot-rich region.[20] Liu et al. fabricated Au rods coated with silica shells and embedded silver nanoparticles for ultrasensitive SERS detection and tunable release of molecules.[21] Our group has previously fabricated a multiscale mesoporous diatom capsule with plasmonic NPs to enable efficient substrate−environment interactions while simultaneously achieving plasmonic-enhanced optical fields.[22] The combination of multiscale materials may contribute multifunctionalities to enable rapid and sensitive vapor detection. Diatom frustules are one pragmatic component. Diatoms are unicellular microalgae found abundantly in nature that possess a hierarchal nanoporous biosilica shell called a frustule. The periodic nanopores within the structure of the frustule forms a naturally occurring photonic crystal with properties similar to rationally designed photonic crystals. Frustules have been integrated with optical biosensors and shown capable of enhancing optical signals,[23,24] particularly SERS.[25−28] The photonic crystal structure of the frustule allows the induction of guided-mode resonance (GMR) within its structure, capable of pairing with the plasmonic resonance of metallic nanoparticles, resulting in stronger electromagnetic fields.[25,29] Beyond optical enhancements, the implementation of mesoporous structures in flow-through applications have been shown to result in rapid equilibration due to the favorable transport of the analyte to the substrate,[30,31] and similarly, the hollow, mesoporous biosilica diatom frustule allows fast diffusion of gases.[32] The integration of frustules into a vapor sensor contributes enhanced optical field and increased analyte interaction for greater sensitivity and shorter response time.

Metallic NPs are easily synthesized and have been used, in many forms, as common optical enhancers for SERS.[33−35] However, the near-field plasmonic field enhancement decays exponentially with distance and analyte molecules not in the immediate vicinity of the NP are not detected.[36] The application of a shell, creating a core−shell NP structure, has been shown to contribute oxidative resistivity, thermal stability, and stronger binding affinities for improved molecular trapping.[37−40] It has been verified by several works that silica shells on NPs, fabricated by the Stöber method, result in a thin porous shell.[41−44] Furthermore, the silica shell can lead to facile immobilization of analytes that do not possess metal-

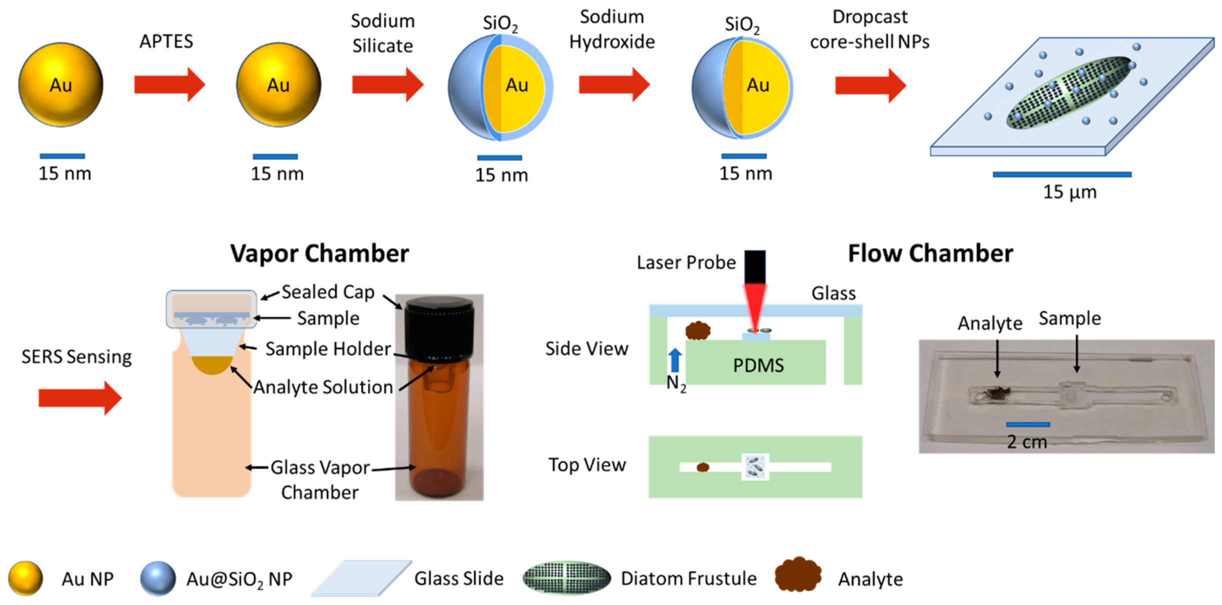

Figure 2. Schematic showing synthesis process of Au@SiO_2 core−shell NPs and subsequent integration on frustule-populated substrate to form multiscale SERS vapor sensor and integration with stagnant vapor and vapor flow chambers.

binding functional groups.[45] This increased binding affinity and large surface area provide abundant binding sites and enable effective analyte trapping and concentration. The multiscale plasmonic NP with a porous shell contributes optical signal enhancement and vapor adsorption capabilities.

The motivation for this work is to create a multiscale SERS substrate capable of sensitive and rapid detection of analyte vapors, particularly explosives. An average of 19 injuries or deaths per day were reported in 2017 worldwide due to exploding land mines with 87% of those being civilians and 47% of the civilians being children.[46] TNT and its byproduct, DNT, are common components found in land mines. Though the percentage of DNT present is small compared to TNT, its vapor pressure is 20−100× greater, making it a preferred indicator for explosive device detection.[47,48] Deteriorated casings of land mines release vaporized explosives into the soil and air, enabling detection. In this work, we present a multiscale vapor SERS sensor, synergistically pairing gold−silica core−shell (Au@SiO_2) nanoparticles and photonic crystal-like frustules for the rapid and sensitive vapor SERS detection of DNT. The 36 nm plasmonic core and the porous, nanometer thick shell enable enhanced electromagnetic fields, while trapping analyte molecules in these sensing regions. Meanwhile, the 30 μm frustule with 200 nm pores enables further field enhancement, as well as improved vapor−substrate interaction, enabling a rapid response. Using numerical methods, we verify the Au@SiO_2 NPs SERS capabilities and the SERS enhancement from diatom. The polycyclic aromatic hydrocarbon pyrene is used as a model molecule to experimentally characterize our multiscale vapor SERS substrate. The contributions from each component of the multiscale sensor are explored, and detection of pyrene vapor at 1 ppm is achieved in only 3 min. DNT vapor is also detected at room temperature below 100 ppb in under 3 min, thus demonstrating the potential of our multiscale sensor for target vapor sensing.

2. THEORETICAL MODELING

To investigate the SERS effect from Au@SiO_2 NPs and the SERS enhancement from diatom frustules, Lumerical's finite-difference time-domain (FDTD) analysis was employed for optical modeling. It is well-known that the plasmonic enhancement from the metallic NP is a near-field effect and is greatly influenced by changes to the refractive index on and near its surface.[49] To determine the SERS capabilities of the Au NP with the presence of a silica shell, two Au@SiO_2 NPs with 36 nm diameter Au cores and a 1 nm thick silica shell were placed 2 nm apart. A 785 nm incident plane wave source was used to replicate our experimental conditions. The source excites the surface plasmons and induces a localized surface plasmon in the gap, or hot spot, between the NPs. It is known that the SERS enhancement is proportional to the fourth power of the amplitude of the electric field ($|E|^4$).[50] As seen in Figure 1a, the plasmonic-enhanced field yields enhanced $|E|^4$ levels as high as 10^5× stronger than the incident source. Therefore, the Au@SiO_2 NP structures yield strong electromagnetic field enhancements, and their utility for SERS is verified.

To investigate the SERS signal enhancement from a diatom, Au@SiO_2 NPs were randomly distributed on a simulant diatom, as seen in Figure 1d, and glass substrates. To enable accurate comparison between the two substrates, the NPs were distributed in the same manner and in the same positions on both substrates. Similar to our previous work,[23] the theoretical diatom was modeled by using a porous silica slab with 160 nm pore diameter, 120 nm pore depth, and 300 nm periodicity. At the bottom of the pores, subpores were modeled as shown in Figure 1d. Matlab was used to randomize NP distribution, in the same configuration on both substrates, and the structure was excited with a 785 nm plane wave. The $|E|^4$ field was calculated on diatom and plotted on a log scale in Figure 1b. The $|E^4|$ field on glass was also calculated, and the SERS enhancement factor (EF) from diatom is determined by eq 1 and is plotted on a logarithmic scale in Figure 1c.

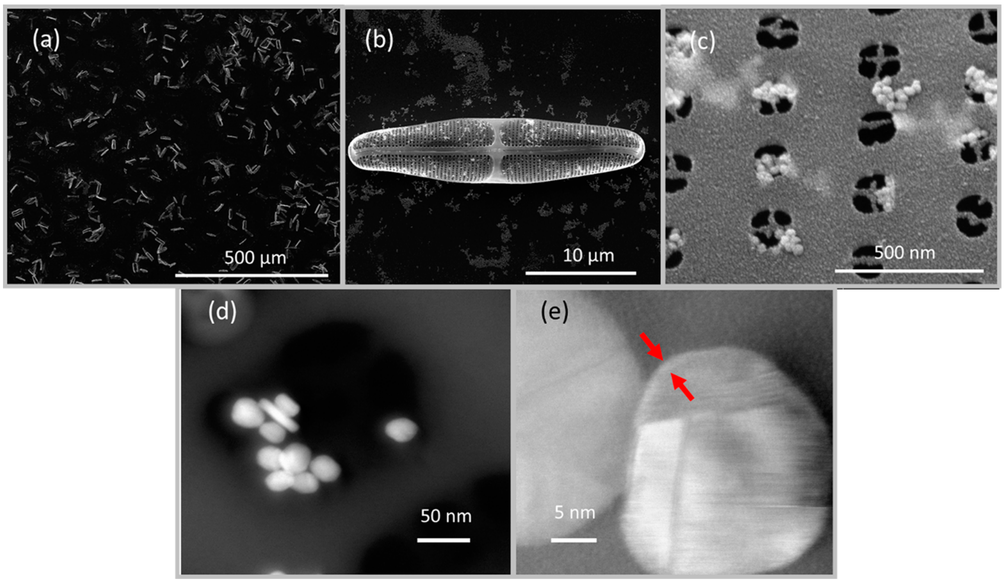

Figure 3. SEM images of the combined multiscale SERS substrate with core−shell and frustule structure shown at different magnifications (a−c). TEM images of NPs in a frustule pore (d) and core−shell structure with arrows highlighting the shell (e).

$$\mathrm{EF} = \left| \frac{{E_{\mathrm{Diatom}}}^4}{{E_{\mathrm{Glass}}}^4} \right| \qquad (1)$$

As can be seen, the EF from diatom enables average SERS enhancements of 10×, with a significant portion of the structure experiencing 100× enhancements and some portion as high as 10^5×. This matches our group's previously measured SERS intensity enhancements.[17,29,51] The large SERS EF can be attributed to the GMR of the photonic crystal-like structure. Incident light upon the diatom surface induces resonant leaky modes within the silica substrate. These resonant modes result in enhanced electromagnetic fields that subsequently interact with the plasmonic NPs. The plasmonic−photonic interaction between the GMR and the plasmonic fields on the NPs results in significantly increased SERS effect and enables greater sensitivity for explosive vapor detection.

3. EXPERIMENTAL SECTION

3.1. Synthesis of Au@SiO$_2$ Nanoparticles. The synthesis of the core−shell nanoparticles follows a procedure similar to the one found in the literature[37] with minor modifications and is shown in the schematic in Figure 2. First, 70 mg of gold chloride was dissolved in 200 mL of water and stirred at 130 °C for 10 min. Next, 8.4 mL of 1% sodium citrate in water (H_2O) (w/w) was slowly added and left stirring for 20 min at 230 °C. During this process, the color changed from a pale yellow to a deep purple, indicating the formation of gold NPs. The gold colloid was allowed to cool, and then NPs were separated into 50 mL aliquots and centrifuged at 7000 rpm for 15 min. The supernatant was removed, and the concentrated NPs were stored at 4 °C for future use. One aliquot was resuspended in 50 mL of H_2O, and the colloidal solution was used to coat with a silica shell. 100 μL of 1 mM (3-aminopropyl)triethoxysilane (APTES) was added to the 20 mL colloidal Au NPs and stirred at room temperature for 20 min to silanate the surface. The pH of the solution was verified to be between 5 and 7 and adjusted if necessary. Sodium silicate solution was diluted in H_2O to 0.54%, and 1 mL of this mixture was slowly pipetted into the mixing solution. This was left vigorously mixing for 20 h to coat the NPs with a silica shell. 1 mL of 0.1 M sodium hydroxide in H_2O was slowly added and stirred gently for 4 h to reduce the shell. The colloidal Au@SiO$_2$ NPs were centrifuged at 6000 rpm for 20 min and resuspended in 20 mL of H_2O. The solution was centrifuged again by using the same conditions, after which it was decanted and left concentrated and stored at 4 °C for future use. NP integration with diatom frustule-populated substrates is detailed in the Supporting Information.

3.2. Vapor Chamber Setup. A vapor chamber, shown in Figure 2, was created by using a glass vial, inset with a sample holder. 20 μL of an analyte−ethanol solution was pipetted into the sample holder, and the multiscale SERS substrate was placed facedown above the solution, high enough to ensure that no solution interacted with the substrate. The chamber was then sealed with thermal tape and Parafilm Sealing Film. The chamber was heated on a hot plate to 70 °C and left for various times. The SERS signal was immediately measured afterward. For each substrate, 20 measurements were made, and the 10 most similar were taken. The average and standard deviation of the characteristic peak intensity were calculated.

3.3. Flow Vapor Chamber. The flow chamber is shown in Figure 2. A $3 \times 60 \times 2$ mm^3 (width × length × height) polydimethylsiloxane channel was constructed with a larger sample holding area (7 × 7 mm^2) in the middle. 10 ± 5 mg of solid explosive DNT was placed near the inlet and about 2 cm away from the sensor. Once the sample and multiscale sensor were placed in the channel, it was sealed with a glass slide. Nitrogen gas flowed through the channel with a regulator pressure of 1 psi. The Raman excitation source was focused through the glass slide and onto the sensor within the channel, and measurements were taken immediately and continuously with 50 mW power and 60 s integration. Before each use, the channel was rinsed with ethanol (EtOH) and H_2O followed by drying with nitrogen gas to ensure its freedom from contaminants.

4. RESULTS AND DISCUSSION

4.1. Au@SiO$_2$ NP Characterization. The Au@SiO$_2$ core−shell NPs were synthesized as described in the Experimental Section. Utilizing scanning electron microscopy (SEM) and transmission electron microscopy (TEM), we characterized the nanoparticles. It was found that the diameter of the NPs was 36 ± 5 nm with a representative SEM and the size distribution being shown in the Figure S1a,b of the Supporting Information. Strong optical absorption was measured, indicating the plasmonic effect of the NPs, which is plotted in Figure S1c. The diatom frustules were prepared as described in the Supporting Information. The diatom frustules are about 30 μm along the major axis and 10 μm along the minor axis

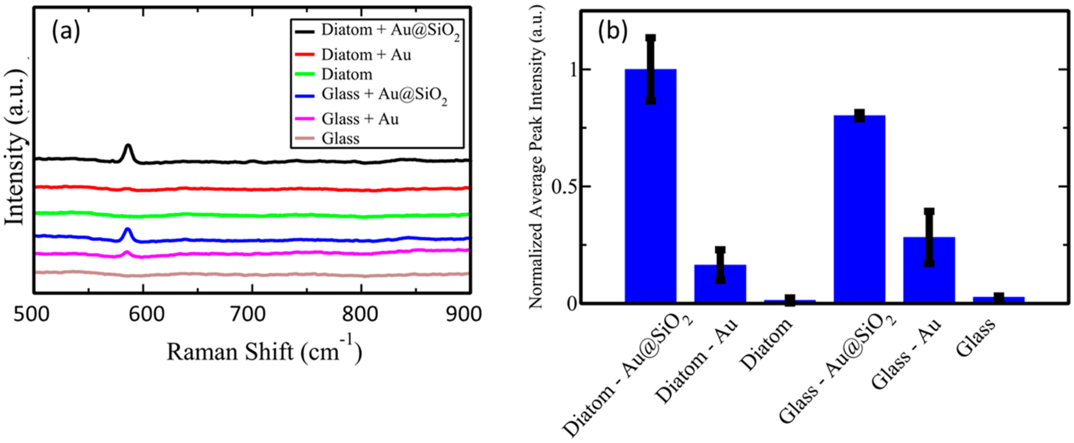

Figure 4. Representative pyrene spectra (100 ppm) on frustule and glass substrates with Au@SiO_2 NPs, Au NPs, or no NPs (a) and bar graph showing normalized average characteristic peak intensities for each substrate (b).

with prime pores and subpores of 200 and 70 nm diameter, respectively. The large surface area-to-volume ratio of the biosilica frustule and the abundant silanol groups on its surface endow the frustule with abundant binding sites allowing for efficient NP decoration. The combination of the core−shell NPs with the micrometer-sized frustules was achieved by using a simple drop-casting method. The resulting macroscopic multiscale hybrid structure is shown in Figure 3a, and the microscopic diatom frustule, showing core−shell NPs within the frustule pores, is shown in Figure 3b,c. Frustules, as has been shown in our previous work, contribute optical field enhancements from GMR which combine with the plasmonic resonance of the nanoparticles. This enhancement is greatest when the plasmonic NPs are within the pores of the frustule.[25,26] The TEM image in Figure 3d verifies the existence of NPs within the pores, ensuring the effective combination of the biosilica diatom frustule and the plasmonic core−shell NPs. The core−shell NP structure is shown in Figure 3e. The metallic core, responsible for the plasmonic enhancement can be seen, as well as the porous shell around it. By use of the TEM image, the shell is confirmed to have a thickness of ∼1 nm, which follows the literature.[37] The nanoparticle composition was further investigated by using energy-dispersive X-ray spectroscopy and is shown in Figure S2. These images verify the formation of the core−shell NPs, their population upon the diatom frustules and in the frustule pores, and finally the total fabrication of our multiscale hybrid SERS substrate.

4.2. Core−Shell NPs for Vapor SERS. Traditional plasmonic NPs are not very effective for vapor SERS sensing due to the poor adsorption of the analyte. A silica shell with increased thickness would allow for greater analyte adsorption within the shell, but the analytes adsorbed onto the surface would be further away from the plasmonic-enhanced field. These two competing factors, greater in-shell analyte adsorption and larger distance of surface-adsorbed analytes from plasmonic-enhanced field, should be balanced to optimize the vapor SERS detection. A shell thickness of 1 nm was chosen as a starting point and may be optimized in future work. The SERS capabilities of the Au@SiO_2NPs were characterized by drop-casting various concentrations of the pyrene−EtOH solution onto the core−shell−frustule substrate and measuring the signal with the results shown in Figure S3. Using the core−shell NPs, we achieved solution-based detection of pyrene down to 100 ppb, showing that the core−shell structure is capable of SERS. Having verified the solution-based SERS capabilities of the core−shell NPs, vapor SERS is investigated. To thoroughly investigate and attribute the contribution from core−shell NPs, we prepared glass substrates with and without diatom frustules and drop-cast (1) Au@SiO_2 NPs, (2) Au NPs, or (3) no NPs onto their surfaces. The substrates were then placed facedown in the stagnant vapor chamber shown in Figure 2 above, with 20 μL of 100 ppm pyrene−ethanol solution as described in the Experimental Section. The substrates were heated for 5 min, and SERS was measured. Representative spectra for each substrate are shown in Figure 4a. The characteristic peak at 587 cm^{-1} is attributed to the CCH out-of-plane deformation and is used in our analysis. The average and standard deviation of the characteristic peak intensity are calculated from 10 spectra and displayed for each substrate in Figure 4b.

When comparing substrates with no NPs, Au NPs, or Au@SiO_2 NPs, the peak intensity is significantly greater when the core−shell structure is employed. This observed SERS improvement can be attributed to the physical enhancement of vapor adsorption and concentration in the shell of the NP. Because the enhanced field effect from the plasmon resonance decays exponentially with distance from the particle, it is desirable to have the analytes as close to the metallic core as possible.[36] The addition of the silica shell and the subsequent hydroxylation of the surface siloxane sites result in the formation of silanol groups (Si−OH) which enables efficient hydrogen bonding between the core−shell NP and the analyte.[52] The improved binding affinity and resulting entrapment of the analyte within the porous shell serves to both concentrate and localize the analyte within close proximity to the plasmon, thus enabling greater interaction with the enhanced field and resulting in the improved sensing.

Comparing the peak intensity on the frustule-populated substrate and that without frustules, we see a relatively small enhancement. This can be attributed to the NP density upon each the substrate. Because of the hydrophilic nature of the frustules, the drop-casted NPs spread further and cover a larger area on diatom substrates than on the glass substrate, resulting in a lower density of NPs, as shown in Figure S4. This will be remedied in future iterations by optimizing parameters such as NP concentration or number of drop-cast repetitions. However, despite the lower NP density, the SERS intensity

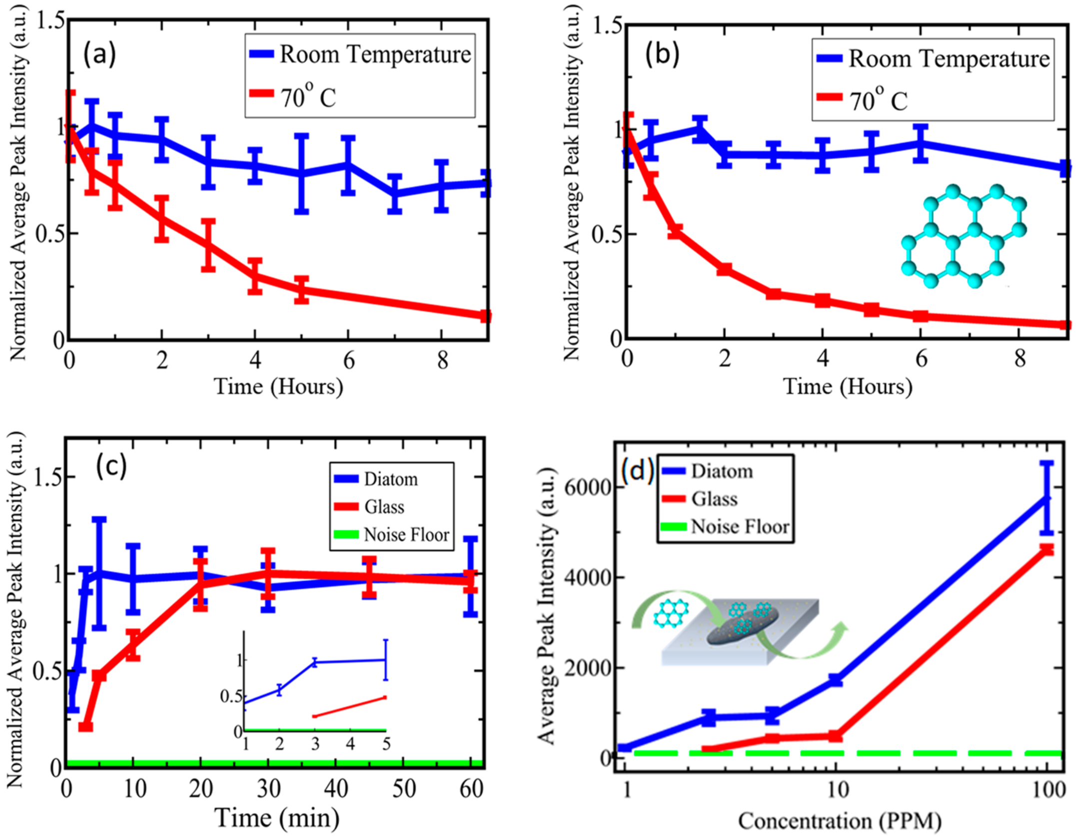

Figure 5. Time-dependent desorption on substrates with (a) and without (b) diatom frustules at room temperature and at 70 °C. A molecular pyrene inset is also shown in (b). The normalized average peak intensity is displayed with respect to time with a zoomed inset (c). Average peak intensity with respect to analyte concentration is plotted to show the concentration dependence with a diatom−vapor interaction schematic inset (d).

on the frustule-populated substrate is still greater than that on glass due to the combination of the plasmonic−photonic enhancements from the pairing of the NPs with diatom frustule.

4.3. 3-Dimensional Biosilica Diatom Frustule Analysis. After validating the utility of the core−shell NPs, we analyzed the enhancements from diatom frustules. To verify the accuracy of our measurement, the time-dependent analyte desorption was measured. Au@SiO_2-populated substrates with and without diatoms were placed in the vapor chamber for 12 h at 70 °C with 20 μL of 100 ppm pyrene in EtOH. SERS measurements were taken immediately following the substrates' removal from the chamber and again at each of the intervals denoted on the plots in Figure 5a,b. Twenty measurements were taken, and the peak intensities were calculated. The 10 spectra with peak intensities closest to the mean were averaged, and the standard deviation was calculated and plotted with respect to time. At room temperature, even after 2 h, the adsorbed molecules remain affixed within our sensor, resulting in little to no change in the SERS intensity. Thus, any desorption of analytes between the sensor's removal from the chamber, and its immediate measurement afterward, is negligible, demonstrating a strong binding affinity between the analyte and the SERS substrate. When 70 °C heat is applied, the desorption of the molecules occurs much more quickly and may be employed for future sensor reuse.

To investigate the reduction of response time due to the presence of diatom frustules, the time-dependent adsorption of frustule and glass substrates was measured. Substrates with Au@SiO_2 NPs were placed in the vapor chamber and heated for various times at 70 °C with 20 μL of pyrene in EtOH. The 20 SERS spectra were measured upon removal from the vapor chamber, and 10 were selected to calculate the average and standard deviation of the characteristic peak at 587 cm^{-1}. The average peak intensity, normalized to the saturation intensity for each substrate, was plotted in Figure 5c. As can be seen from the plots below, the diatom-based sensor has a much faster response time, reaching equilibrium within 3 min, whereas the substrate without diatoms has almost no signal at 3 min and took 20 min to equilibrate. This 6-fold reduction in response time can be attributed to the mesoporous structure of the diatom frustule. The porous 3D frustule allows the analyte vapor to rapidly permeate the structure and have greater interaction with the core−shell NPs compared to those decorating the planar glass surface. This results in rapid analyte adsorption into the porous shell of the NPs and thus faster detection and saturation times. This effect has been utilized previously with the implementation of mesoporous structures in flow-through sensing applications resulting in rapid equilibration due to the favorable transport of the analyte to the substrate.[30,31] Similarly, the hollow, mesoporous biosilica diatom frustule has demonstrated fast diffusion of gases.[32] The utilization of the 3D porous frustule in our application enables efficient vapor−substrate interaction and, consequentially, rapid adsorption and concentration within the porous NP shell.

The dependence of the SERS peak intensity to the analyte concentration was compared between the frustule-populated

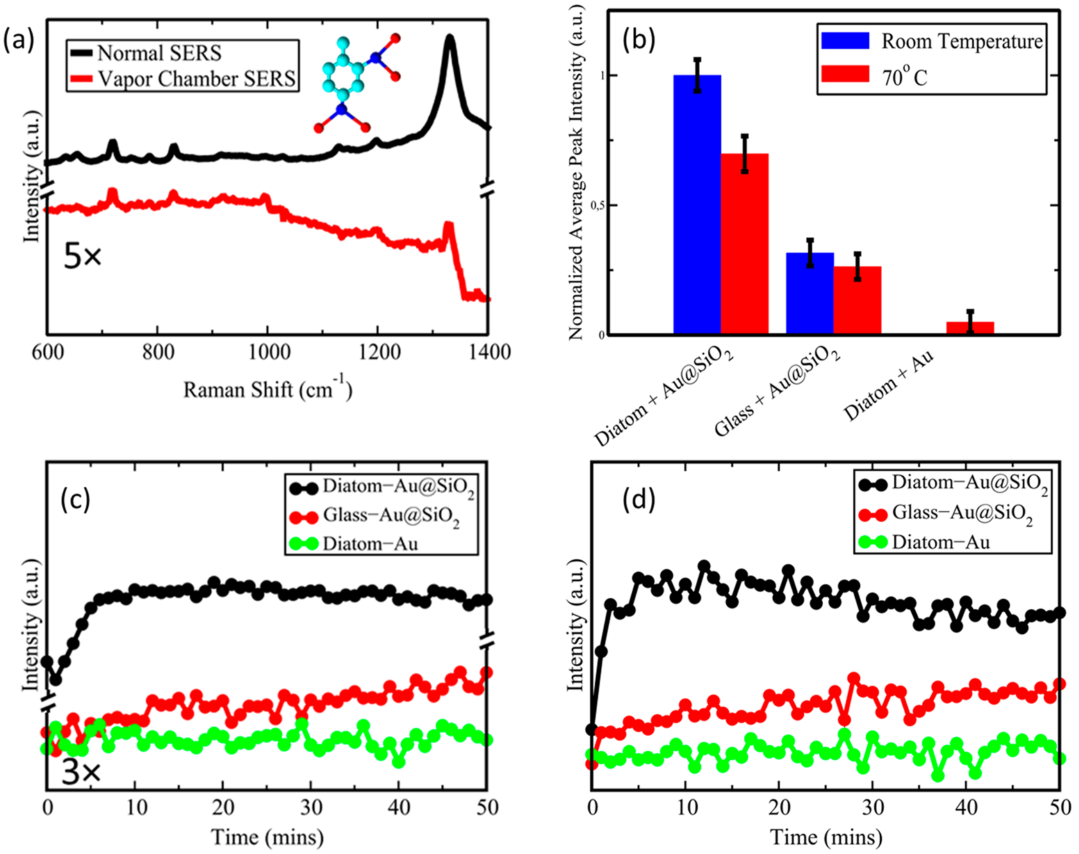

Figure 6. Regular and vapor chamber SERS spectra are shown with the molecular structure of DNT inset (a). Average characteristic peak intensity on diatom−Au@SiO$_2$, glass−Au@SiO$_2$, and diatom−Au substrates in DNT flow chamber at room temperature and at 70 °C are shown (b). The time dependence is also shown at room temperature (c) and at 70 °C (d). Different scales are used to highlight trends and peaks (a, c).

substrate and the regular glass substrate. Using the same vapor chamber setup and various concentrations of pyrene in EtOH heated for 5 min, we obtained the results shown in Figure 5d. The noise floor was defined to be the average characteristic peak intensity of the control substrate (no pyrene present) plus 3 times its standard deviation. As can be seen from the plot, detection without diatom was achieved down to 2.5 ppm, whereas concentrations down to 1 ppm were obtained with frustules. It has been shown that guided resonant modes can be excited within the photonic crystal-like structure of the diatom frustule and result in enhanced SERS sensitivity.[25,28] The guided resonant mode interacts with the plasmonic resonance from the core−shell NPs to achieve a plasmonic−photonic enhancement capable of inducing fields over 20 times greater than those from metal nanoparticles on planar glass.[29] Additionally, as seen in Figure 5d, the enhancement factor from diatom increases with a decrease in analyte concentration. This is evidence of the further enhancement from the 3D frustule structure. At higher concentrations with an abundance of analytes, natural diffusion is sufficient for effective analyte interaction with the core−shell NPs. However, at lower concentrations, the 3D structure is indispensable to allow efficient interaction of analyte molecules with the NPs. This accounts for the difference between the small enhancement from diatom seen in Figure 4b at high analyte concentration and the large diatom enhancement seen at lower concentrations in Figure 5d. The reproducibility of the sensor was also verified by performing an experiment in triplicate. The experimental details and results are shown in Figure S5, and the average characteristic peak intensities are within 10% between the three samples, demonstrating high reproducibility.

4.4. Application of Multiscale SERS Substrate for DNT Detection.

By use of the multiscale SERS substrate, DNT was detected in the vapor chamber shown in Figure 2 and described in the Experimental Section. The substrate was placed facedown above 20 mg of solid DNT, and the chamber was heated for 30 min. Figure 6a shows the 1000 ppm solution-based DNT SERS spectrum as well as the background-subtracted vapor SERS spectrum. The main characteristic peaks at 830 and 1332 cm^{-1} correspond to the out-of-plane NO$_2$ bending mode and the NO$_2$ stretching mode, respectively. The background subtraction in the vapor SERS measurement resulted in a slight baseline decrease at higher wavenumbers due to the background fluorescence fluctuation. However, both characteristic peaks are clearly detectable, demonstrating the ability to sense DNT in the stationary vapor chamber.

The detection of DNT in a sealed container where a saturated headspace can form was performed to verify the detection capabilities; however, it is desirable to create a sensor capable of detecting buried land mines in their environment, without the need for the formation of a concentrated headspace. The practical detection of DNT is achieved by utilizing a flow chamber as shown in Figure 2 and described in the Experimental Section. The concentration of DNT in this setup is less than the saturation vapor (100 ppb) and simulates real detection conditions where an equilibrated headspace may not have formed due to ambient air flow. For this detection, 10

https://dx.doi.org/10.1021/acsanm.9b02399
ACS Appl. Nano Mater. XXXX, XXX, XXX−XXX

± 0.5 mg of DNT was placed 2 cm away from the substrate and nitrogen flowed through the chamber over the DNT and the multiscale SERS substrate. SERS signals were measured continuously. Using this setup, we tested diatom−Au@SiO_2 NP, diatom−Au NP, and glass−Au@SiO_2 NP substrates. This was done at room temperature as well as under heating conditions at 70 °C. The normalized average peak intensity of the 1332 cm^{-1} peak for each of these, along with their standard deviation, is shown in Figure 6b. As can be seen, the intensity on the substrate with diatom frustules and core−shell NPs at room temperature yields the best results, while the diatom−Au NP substrate shows almost no signal and the glass−Au@SiO_2 NP substrate shows a very slow response. This agrees with our previous pyrene characterization and highlights the importance of the core−shell and 3D frustule structures. Comparing temperature, one may expect the signal to be stronger under heated circumstances as that allows for more DNT to vaporize. While true, the heating condition also allows for trapped analytes within the core−shell structure to dissociate more quickly, as shown by our time-dependent desorption analysis in Figure 5a,b. The stronger SERS intensity at room temperature is advantageous, as detection can be achieved without the need of external heating.

In addition to investigating the average peak intensity, we measured the time-dependent intensity at room temperature and 70 °C (Figure 6c,d). From these plots, it is clear that the diatom−core−shell hybrid substrate yields the best results with the highest intensity and fastest response time. The diatom−Au NP substrate shows almost no signal. The glass−Au@SiO_2 NP substrate shows a clear signal; however, even after 50 min the substrate still has not reached equilibrium sensitivity. On the other hand, the multiscale diatom−Au@SiO_2 NP substrate has a strong signal, capable of detecting the vapor within 3 min and reaching equilibrated response within only 5 min, allowing for fast and sensitive measurements. The performances of the diatom−Au NP and glass−Au@SiO_2 NP substrates are similar under heated conditions as those at room temperature. However, the diatom−core−shell NP substrate shows a faster response time of 1 min and saturates within 3 min, but with a slightly lower intensity due to the dissociation of the trapped analyte. The collaborative contributions from photonic crystal-like diatom frustules and core−shell Au@SiO_2 NPs coalesce in this detection of DNT. The multiscale nature of our sensor enables rapid response while enhancing the analyte signal compared to other substrates. This clearly highlights both the ability of our sensor for vapor-based explosives sensing and its potential for further applications.

5. CONCLUSION

In this work, we have demonstrated a multiscale SERS substrate by synergistically combining naturally occurring photonic crystal-like diatom frustules and Au NPs with a mesoporous silica shell and used this substrate for the detection of explosive vapor. Utilizing a custom vapor chamber and the model analyte pyrene, we verified the contributions from each component of the multiscale substrate. The nanometer thick porous silica shell traps and concentrates the analyte vapor while the 36 nm plasmonic core enhances the Raman signal. The periodic array of 70 nm wide subpores and 200 nm wide prime pores of the 30 μm long diatom frustule enables GMR that couples with the plasmonic resonance of the NP for more sensitive SERS. The largely hollow and porous structure of the frustule allows for greater circulation and improved vapor−substrate interactions. These functionalities were employed using a flow chamber and detection of DNT vapor from the solid explosive below 100 ppb was demonstrated within 3 min at room temperature with the sensor reaching equilibrium in only 5 min. The sensitive and rapid detection results achieved by this multiscale SERS substrate clearly illustrate its capabilities for vapor-phase explosives detection and its potential for future land mine and other vapor-phase SERS detections.

■ ASSOCIATED CONTENT

Supporting Information

The Supporting Information is available free of charge at https://pubs.acs.org/doi/10.1021/acsanm.9b02399.

Further details regarding the materials used, the synthesis of the multiscale SERS substrate, and characterization (PDF)

■ AUTHOR INFORMATION

Corresponding Author

Alan X. Wang − *School of Electrical Engineering and Computer Science, Oregon State University, Corvallis, Oregon 97331, United States;* orcid.org/0000-0002-0553-498X; Email: wang@oregonstate.edu

Authors

Kenneth J. Squire − *School of Electrical Engineering and Computer Science, Oregon State University, Corvallis, Oregon 97331, United States*

Kundan Sivashanmugan − *School of Electrical Engineering and Computer Science, Oregon State University, Corvallis, Oregon 97331, United States*

Boxin Zhang − *School of Electrical Engineering and Computer Science, Oregon State University, Corvallis, Oregon 97331, United States*

Joseph Kraai − *School of Chemical, Biological & Environmental Engineering, Oregon State University, Corvallis, Oregon 97331, United States*

Gregory Rorrer − *School of Chemical, Biological & Environmental Engineering, Oregon State University, Corvallis, Oregon 97331, United States*

Complete contact information is available at:
https://pubs.acs.org/10.1021/acsanm.9b02399

Notes

The authors declare no competing financial interest.

■ ACKNOWLEDGMENTS

The authors acknowledge the support from the National Science Foundation under Grant 1701329, the National Institutes of Health under Grant 1R21DA0437131, and the Unites States Department of Agriculture under Grant 2017-67021-26606.

■ REFERENCES

(1) Kneipp, K.; Wang, Y.; Kneipp, H.; Perelman, L. T.; Itzkan, I.; Dasari, R. R.; Feld, M. S. Single Molecule Detection Using Surface-Enhanced Raman Scattering (SERS). *Phys. Rev. Lett.* **1997**, *78* (9), 1667−1670.

(2) Zhang, D.; Huang, L.; Liu, B.; Ge, Q.; Dong, J.; Zhao, X. Rapid and Ultrasensitive Quantification of Multiplex Respiratory Tract Infection Pathogen via Lateral Flow Microarray based on SERS Nanotags. *Theranostics* **2019**, *9* (17), 4849−4859.

(3) Kodiyath, R.; Malak, S. T.; Combs, Z. A.; Koenig, T.; Mahmoud, M. A.; El-Sayed, M. A.; Tsukruk, V. V. Assemblies of silver nanocubes for highly sensitive SERS chemical vapor detection. *J. Mater. Chem. A* **2013**, *1* (8), 2777−2788.

(4) Kreno, L. E.; Greeneltch, N. G.; Farha, O. K.; Hupp, J. T.; Van Duyne, R. P. SERS of molecules that do not adsorb on Ag surfaces: a metal−organic framework-based functionalization strategy. *Analyst* **2014**, *139* (16), 4073−4080.

(5) Taranenko, N.; Alarie, J.-P.; Stokes, D. L.; Vo-Dinh, T. Surface-Enhanced Raman Detection of Nerve Agent Simulant (DMMP and DIMP) Vapor on Electrochemically Prepared Silver Oxide Substrates. *J. Raman Spectrosc.* **1996**, *27* (5), 379−384.

(6) Phan-Quang, G. C.; Yang, N.; Lee, H. K.; Sim, H. Y. F.; Koh, C. S. L.; Kao, Y.-C.; Wong, Z. C.; Tan, E. K. M.; Miao, Y.-E; Fan, W.; Liu, T.; Phang, I. Y.; Ling, X. Y. Tracking Airborne Molecules from Afar: Three-Dimensional Metal-Organic-Framework - Surface-Enhanced Raman Scattering (MOF-SERS) Platform for Stand-Off and Real-Time Atmospheric Monitoring. *ACS Nano* **2019**, *13* (10), 12090−12099.

(7) Muehlethaler, C.; Leona, M.; Lombardi, J. R. Review of Surface Enhanced Raman Scattering Applications in Forensic Science. *Anal. Chem.* **2016**, *88* (1), 152−169.

(8) Chou, A.; Jaatinen, E.; Buividas, R.; Seniutinas, G.; Juodkazis, S.; Izake, E. L.; Fredericks, P. M. SERS substrate for detection of explosives. *Nanoscale* **2012**, *4* (23), 7419−7424.

(9) Khaing Oo, M. K.; Chang, C.-F.; Sun, Y.; Fan, X. Rapid, sensitive DNT vapor detection with UV-assisted photo-chemically synthesized gold nanoparticle SERS substrates. *Analyst* **2011**, *136* (13), 2811−2817.

(10) Khaing Oo, M. K.; Guo, Y.; Reddy, K.; Liu, J.; Fan, X. Ultrasensitive Vapor Detection with Surface-Enhanced Raman Scattering-Active Gold Nanoparticle Immobilized Flow-Through Multihole Capillaries. *Anal. Chem.* **2012**, *84* (7), 3376−3381.

(11) Piorek, B. D.; Lee, S. J.; Moskovits, M.; Meinhart, C. D. Free-Surface Microfluidics/Surface-Enhanced Raman Spectroscopy for Real-Time Trace Vapor Detection of Explosives. *Anal. Chem.* **2012**, *84* (22), 9700−9705.

(12) Demeritte, T.; Kanchanapally, R.; Fan, Z.; Singh, A. K.; Senapati, D.; Dubey, M.; Zakar, E.; Ray, P. C. Highly efficient SERS substrate for direct detection of explosive TNT using popcorn-shaped gold nanoparticle-functionalized SWCNT hybrid. *Analyst* **2012**, *137* (21), 5041−5045.

(13) Wang, J.; Yang, L.; Boriskina, S.; Yan, B.; Reinhard, B. M. Spectroscopic Ultra-Trace Detection of Nitroaromatic Gas Vapor on Rationally Designed Two-Dimensional Nanoparticle Cluster Arrays. *Anal. Chem.* **2011**, *83* (6), 2243−2249.

(14) Sylvia, J. M.; Janni, J. A.; Klein, J. D.; Spencer, K. M. Surface-Enhanced Raman Detection of 2,4-Dinitrotoluene Impurity Vapor as a Marker To Locate Landmines. *Anal. Chem.* **2000**, *72* (23), 5834−5840.

(15) Ko, H.; Chang, S.; Tsukruk, V. V. Porous Substrates for Label-Free Molecular Level Detection of Nonresonant Organic Molecules. *ACS Nano* **2009**, *3* (1), 181−188.

(16) Cho, S.-Y.; Kim, S. J.; Lee, Y.; Kim, J.-S.; Jung, W.-B.; Yoo, H.-W.; Kim, J.; Jung, H.-T. Highly Enhanced Gas Adsorption Properties in Vertically Aligned MoS2 Layers. *ACS Nano* **2015**, *9* (9), 9314−9321.

(17) Kong, X.; Xi, Y.; LeDuff, P.; Li, E.; Liu, Y.; Cheng, L.-J.; Rorrer, G. L.; Tan, H.; Wang, A. X. Optofluidic sensing from inkjet-printed droplets: the enormous enhancement by evaporation-induced spontaneous flow on photonic crystal biosilica. *Nanoscale* **2016**, *8* (39), 17285−17294.

(18) Zhang, H.; Liu, M.; Zhou, F.; Liu, D.; Liu, G.; Duan, G.; Cai, W.; Li, Y. Physical Deposition Improved SERS Stability of Morphology Controlled Periodic Micro/Nanostructured Arrays Based on Colloidal Templates. *Small* **2015**, *11* (7), 844−853.

(19) Liu, B.; Zhang, D.; Ni, H.; Wang, D.; Jiang, L.; Fu, D.; Han, X.; Zhang, C.; Chen, H.; Gu, Z.; Zhao, X. Multiplex Analysis on a Single Porous Hydrogel Bead with Encoded SERS Nanotags. *ACS Appl. Mater. Interfaces* **2018**, *10* (1), 21−26.

(20) Li, H.; Yang, Q.; Hou, J.; Li, Y.; Li, M.; Song, Y. Bioinspired Micropatterned Superhydrophilic Au-Areoles for Surface-Enhanced Raman Scattering (SERS) Trace Detection. *Adv. Funct. Mater.* **2018**, *28* (21), 1800448.

(21) Liu, J.; Guo, J.; Meng, G.; Fan, D. Superstructural Raman Nanosensors with Integrated Dual Functions for Ultrasensitive Detection and Tunable Release of Molecules. *Chem. Mater.* **2018**, *30* (15), 5256−5263.

(22) Sivashanmugan, K.; Squire, K.; Kraai, J. A.; Tan, A.; Zhao, Y.; Rorrer, G. L.; Wang, A. X. Biological Photonic Crystal-Enhanced Plasmonic Mesocapsules: Approaching Single-Molecule Optofluidic-SERS Sensing. *Adv. Opt. Mater.* **2019**, *7* (13), 1900415.

(23) Squire, K.; Kong, X.; LeDuff, P.; Rorrer, G. L.; Wang, A. X. Photonic crystal enhanced fluorescence immunoassay on diatom biosilica. *Journal of Biophotonics* **2018**, *11* (10), No. e201800009.

(24) Squire, K. J.; Zhao, Y.; Tan, A.; Sivashanmugan, K.; Kraai, J. A.; Rorrer, G. L.; Wang, A. X. Photonic crystal-enhanced fluorescence imaging immunoassay for cardiovascular disease biomarker screening with machine learning analysis. *Sens. Actuators, B* **2019**, *290*, 118−124.

(25) Kong, X.; Squire, K.; Li, E.; LeDuff, P.; Rorrer, G. L.; Tang, S.; Chen, B.; McKay, C. P.; Navarro-Gonzalez, R.; Wang, A. X. Chemical and Biological Sensing Using Diatom Photonic Crystal Biosilica With In-Situ Growth Plasmonic Nanoparticles. *IEEE Transactions on NanoBioscience* **2016**, *15* (8), 828−834.

(26) Kong, X.; Xi, Y.; Le Duff, P.; Chong, X.; Li, E.; Ren, F.; Rorrer, G. L.; Wang, A. X. Detecting explosive molecules from nanoliter solution: A new paradigm of SERS sensing on hydrophilic photonic crystal biosilica. *Biosens. Bioelectron.* **2017**, *88*, 63−70.

(27) Yang, J.; Zhen, L.; Ren, F.; Campbell, J.; Rorrer, G. L.; Wang, A. X. Ultra-sensitive immunoassay biosensors using hybrid plasmonic-biosilica nanostructured materials. *Journal of Biophotonics* **2015**, *8* (8), 659−667.

(28) Chamuah, N.; Chetia, L.; Zahan, N.; Dutta, S.; Ahmed, G. A.; Nath, P. A naturally occurring diatom frustule as a SERS substrate for the detection and quantification of chemicals. *J. Phys. D: Appl. Phys.* **2017**, *50* (17), 175103.

(29) Ren, F.; Campbell, J.; Wang, X.; Rorrer, G. L.; Wang, A. X. Enhancing surface plasmon resonances of metallic nanoparticles by diatom biosilica. *Opt. Express* **2013**, *21* (13), 15308−15313.

(30) Davis, S. C.; Sheppard, V. C.; Begum, G.; Cai, Y.; Fang, Y.; Berrigan, J. D.; Kröger, N.; Sandhage, K. H. Rapid Flow-Through Biocatalysis with High Surface Area, Enzyme-Loaded Carbon and Gold-Bearing Diatom Frustule Replicas. *Adv. Funct. Mater.* **2013**, *23* (36), 4611−4620.

(31) Tortajada, M.; Ramón, D.; Beltrán, D.; Amorós, P. Hierarchical bimodal porous silicas and organosilicas for enzyme immobilization. *J. Mater. Chem.* **2005**, *15* (35−36), 3859−3868.

(32) Lettieri, S.; Setaro, A.; De Stefano, L.; De Stefano, M.; Maddalena, P. The Gas-Detection Properties of Light-Emitting Diatoms. *Adv. Funct. Mater.* **2008**, *18* (8), 1257−1264.

(33) Ding, S.-Y.; Yi, J.; Li, J.-F.; Ren, B.; Wu, D.-Y.; Panneerselvam, R.; Tian, Z.-Q. Nanostructure-based plasmon-enhanced Raman spectroscopy for surface analysis of materials. *Nat. Rev. Mater.* **2016**, *1* (6), 16021.

(34) Zhang, T.; Sun, Y.; Hang, L.; Li, H.; Liu, G.; Zhang, X.; Lyu, X.; Cai, W.; Li, Y. Periodic Porous Alloyed Au−Ag Nanosphere Arrays and Their Highly Sensitive SERS Performance with Good Reproducibility and High Density of Hotspots. *ACS Appl. Mater. Interfaces* **2018**, *10* (11), 9792−9801.

(35) Zhang, H.; Zhou, F.; Liu, M.; Liu, D.; Men, D.; Cai, W.; Duan, G.; Li, Y. Spherical Nanoparticle Arrays with Tunable Nanogaps and Their Hydrophobicity Enhanced Rapid SERS Detection by Localized Concentration of Droplet Evaporation. *Adv. Mater. Interfaces* **2015**, *2* (9), 1500031.

(36) Bharadwaj, P.; Anger, P.; Novotny, L. Nanoplasmonic enhancement of single-molecule fluorescence. *Nanotechnology* **2007**, *18* (4), 044017.

(37) Quyen, T. T. B.; Su, W.-N.; Chen, K.-J.; Pan, C.-J.; Rick, J.; Chang, C.-C.; Hwang, B.-J. Au@SiO$_2$ core/shell nanoparticle assemblage used for highly sensitive SERS-based determination of glucose and uric acid. *J. Raman Spectrosc.* **2013**, *44* (12), 1671−1677.

(38) Liu, Y.; Tang, Z. Multifunctional Nanoparticle@MOF Core−Shell Nanostructures. *Adv. Mater.* **2013**, *25* (40), 5819−5825.

(39) Mueller, M.; Tebbe, M.; Andreeva, D. V.; Karg, M.; Alvarez Puebla, R. A.; Pazos Perez, N.; Fery, A. Large-Area Organization of pNIPAM-Coated Nanostars as SERS Platforms for Polycyclic Aromatic Hydrocarbons Sensing in Gas Phase. *Langmuir* **2012**, *28* (24), 9168−9173.

(40) Ma, L.; Wu, H.; Huang, Y.; Zou, S.; Li, J.; Zhang, Z. High-Performance Real-Time SERS Detection with Recyclable Ag Nanorods@HfO2 Substrates. *ACS Appl. Mater. Interfaces* **2016**, *8* (40), 27162−27168.

(41) Lu, Y.; McLellan, J.; Xia, Y. Synthesis and Crystallization of Hybrid Spherical Colloids Composed of Polystyrene Cores and Silica Shells. *Langmuir* **2004**, *20* (8), 3464−3470.

(42) Nikolić, M. P.; Giannakopoulos, K. P.; Srdić, V. V. Synthesis and characterization of mesoporous and superparamagnetic bilayered-shell around silica core particles. *Ceram. Int.* **2015**, *41* (10), 13480−13485.

(43) Song, C.; Chen, J.; Abell, J. L.; Cui, Y.; Zhao, Y. Ag−SiO$_2$ Core−Shell Nanorod Arrays: Morphological, Optical, SERS, and Wetting Properties. *Langmuir* **2012**, *28* (2), 1488−1495.

(44) Walcarius, A.; Despas, C.; Bessière, J. Molecular sieving with amorphous monodisperse silica beads. *Microporous Mesoporous Mater.* **1998**, *23* (5), 309−313.

(45) Wang, C.; Chen, Y.; Wang, T.; Ma, Z.; Su, Z. Monodispersed Gold Nanorod-Embedded Silica Particles as Novel Raman Labels for Biosensing. *Adv. Funct. Mater.* **2008**, *18* (2), 355−361.

(46) Landmine Monitor 2018; http://www.the-monitor.org/en-gb/reports/2018/landmine-monitor-2018/preface.aspx (accessed 9/5/2019).

(47) Rose, A.; Zhu, Z.; Madigan, C. F.; Swager, T. M.; Bulović, V. Sensitivity gains in chemosensing by lasing action in organic polymers. *Nature* **2005**, *434* (7035), 876−879.

(48) George, V.; Jenkins, T. F.; Leggett, D. C.; Cragin, J. H.; Phelan, J. M.; Oxley, J. C.; Pennington, J. Progress on determining the vapor signature of a buried land mine. *Proc. SPIE* **1999**, *3710*, 258.

(49) Amendola, V.; Pilot, R.; Frasconi, M.; Maragò, O. M.; Iatì, M. A. Surface plasmon resonance in gold nanoparticles: a review. *J. Phys.: Condens. Matter* **2017**, *29* (20), 203002.

(50) Aikens, C. M.; Madison, L. R.; Schatz, G. C. The effect of field gradient on SERS. *Nat. Photonics* **2013**, *7*, 508.

(51) Ren, F.; Campbell, J.; Rorrer, G. L.; Wang, A. X. Surface-Enhanced Raman Spectroscopy Sensors From Nanobiosilica With Self-Assembled Plasmonic Nanoparticles. *IEEE J. Sel. Top. Quantum Electron.* **2014**, *20* (3), 127−132.

(52) Tsendra, O.; Scott, A. M.; Gorb, L.; Boese, A. D.; Hill, F. C.; Ilchenko, M. M.; Leszczynska, D.; Leszczynski, J. Adsorption of Nitrogen-Containing Compounds on the (100) α-Quartz Surface: Ab Initio Cluster Approach. *J. Phys. Chem. C* **2014**, *118* (6), 3023−3034.

https://dx.doi.org/10.1021/acsanm.9b02399